ASEPS-0 Testbed Interferometer

M. M. Colavita, M. Shao, B. E. Hines, J. K. Wallace,
Y. Gursel, F. Malbet, J. W. Yu, H. Singh, C. A. Beichman

Jet Propulsion Laboratory
California Institute of Technology

X. P. Pan, T. Nakajima, S. R. Kulkarni

California Institute of Technology

ABSTRACT

The ASEPS-0 Testbed Interferometer is a long-baseline infrared interferometer optimized for high-accuracy narrow-angle astrometry. It is being constructed by JPL for NASA as a testbed for the future Keck Interferometer to demonstrate the technology for the astrometric detection of exoplanets from the ground. Recent theoretical and experimental work has shown that extremely high accuracy narrow-angle astrometry, at the level of tens of microarcseconds in an hour of integration time, can be achieved with a long-baseline interferometer measuring closely-spaced pairs of stars. A system with performance close to these limits could conduct a comprehensive search for Jupiter- and Saturn-mass planets around stars of all spectral types, and for short-period Uranus-mass planets around nearby M and K stars. The key features of an instrument which can achieve this accuracy are long baselines to minimize atmospheric and photon-noise errors, a dual-star feed to route the light from two separate stars to two beam combiners, cophased operation using an infrared fringe detector to increase sensitivity in order to locate reference stars near a bright target, and laser metrology to monitor systematic errors. The ASEPS-0 Testbed Interferometer will incorporate these features, with a nominal baseline of 100 m, 50-cm siderostats, and 40-cm telescopes at the input to the dual-star feeds. The fringe detectors will operate at 2.2 μm, using NICMOS-III arrays in a fast-readout mode controlling high-speed laser-monitored delay lines. Development of the interferometer is in progress, with installation at Palomar Mountain planned to begin in 1994.

1. INTRODUCTION

Recent theoretical and experimental work on the limitations of narrow-angle differential astrometry from the ground have revealed that the fundamental limitations attributable to atmospheric turbulence are far smaller than had been generally assumed.[1] The key point is that for differential measurements between closely-spaced stars, there is a significant improvement in astrometric accuracy with increasing baseline length. More precisely, one can define the isokinetic angle θ_k as B/h, where B is the instrument baseline (for an interferometer) or diameter (for a single telescope) and h is a mean atmospheric height. For star separations $\theta > \theta_k$, one finds that the astrometric error is only weakly dependent on the star separation and baseline length. In this regime, which is standard for conventional narrow-angle astrometry, errors of a few mas(milliarcsec)/$\sqrt{\text{h}}$ are typical. However, in the regime $\theta < \theta_k$, the dependencies of the error change significantly, and the error improves linearly with decreasing star separation, and with increasing baseline as $B^{2/3}$. This behavior is shown more clearly in Fig. 1, adapted from the previous reference,[1] which plots the error in a 1-hr differential measurement for a range of star separations and baseline lengths for seeing of 0.5 and 1.0 arcsec.

Recently, measurements with the Mark III interferometer at Mt. Wilson were conducted to generate experimental data in the very-narrow-angle regime.[2] The 3.3-arcsec visual binary α Gem was observed on the Mark III's 12-m astrometric baseline. The instrument was modified by dividing the pupil into two halves with separate detectors, and using a pair of tilting plates in one half of the pupil as a differential delay line in order to detect fringes simultaneously on both components of the binary. The data showed that the measured error behaved as white noise out to a measurement limit of 8 min, and that the error, extrapolated to a 1-hr integration time, ranged from 15–25 μas(microarcsec). This behavior, as plotted on Fig. 1, is consistent with the predictions of the theory. With 100 m baselines, this same accuracy should be achieved for star separations of 14 arcsec.

0-8194-1495-6/94/$6.00

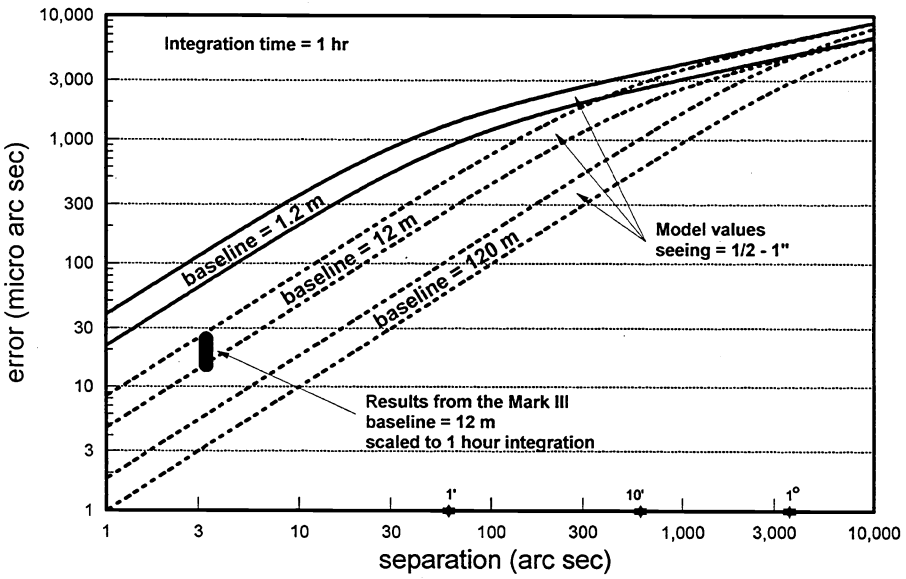

Figure 1: Accuracy of a narrow-angle differential astrometric measurement

This projected performance is quite exciting with regard to the scientific goal of the astrometric detection of exoplanets from the ground. The canonical exoplanet signature is ±0.5 mas for a Jupiter-Sun system at 10 pc, which is too small to be reliably detected with conventional astrometric techniques. However, with the performance available with an instrumental baseline of ~100 m, and a star separation of 15–20 arcsec, deep searches for Jupiter- and Saturn-mass planets could be conducted, in addition to limited searches for lower-mass planets. The features of an instrument which can reach these atmospheric limits are discussed elsewhere;[1] in summary: long-baselines to reduce atmospheric errors; infrared observations for high sensitivity and the larger infrared isoplanatic patch; phase referencing, whereby measurements of the bright target star are used to cophase the instrument within the isoplanatic patch in order to increase sensitivity to find nearby reference stars; and laser metrology to control systematic error in order to reach the atmospheric limits.

The NASA ASEPS (Astronomical Studies of Extrasolar Planetary Systems) program, part of the larger PSS (Planetary Systems Science) program, has among its science objectives the detection and characterization of extrasolar planetary systems with ground- and space-based instruments. A key component of the ground-based program would be an interferometer employing the two Keck telescopes with additional smaller outrigger telescopes. In preparation for this powerful instrument, NASA has funded the ASEPS-0 Testbed Interferometer to demonstrate the technology for narrow-angle interferometric astrometry.

2. TESTBED OVERVIEW

The ASEPS-0 testbed is a long-baseline interferometer optimized for narrow-angle astrometry using phase-referencing. It is presently under development at JPL for installation at Palomar Mountain, California. The design of the testbed draws upon our experience with the Mark III interferometer at Mt. Wilson.[3,4] The basic instrument is a two-element interferometer with a maximum baseline of 100 m. Fringe measurements are at 2.2 μm (K band), with angle tracking at 0.8 μm. Full fringe tracking is implemented using active delay lines. The aperture size is 40 cm, which is a good match to r_0 at 2.2 μm—50 cm for 1 arcsec seeing—and is ~3 r_0 at 0.8 μm for angle tracking. The delay range is ±40 m, providing a worst-case zenith limit of 24 degrees. The system employs two beam combiners: one for fringe tracking on the bright primary star (target), and one phase-referenced to the primary star for detection of the faint secondary star (reference). A laser metrology system monitors the entire optical train to control systematic errors.

The instrument will be installed at Palomar Mountain, California. Figure 2 shows the planned layout at Palomar; the instrument will be located north-east of the 5-m Hale telescope. The figure shows 6 possible pier locations, although for demonstration purposes, a single wide pair will suffice. Maximum baselines on this diagram

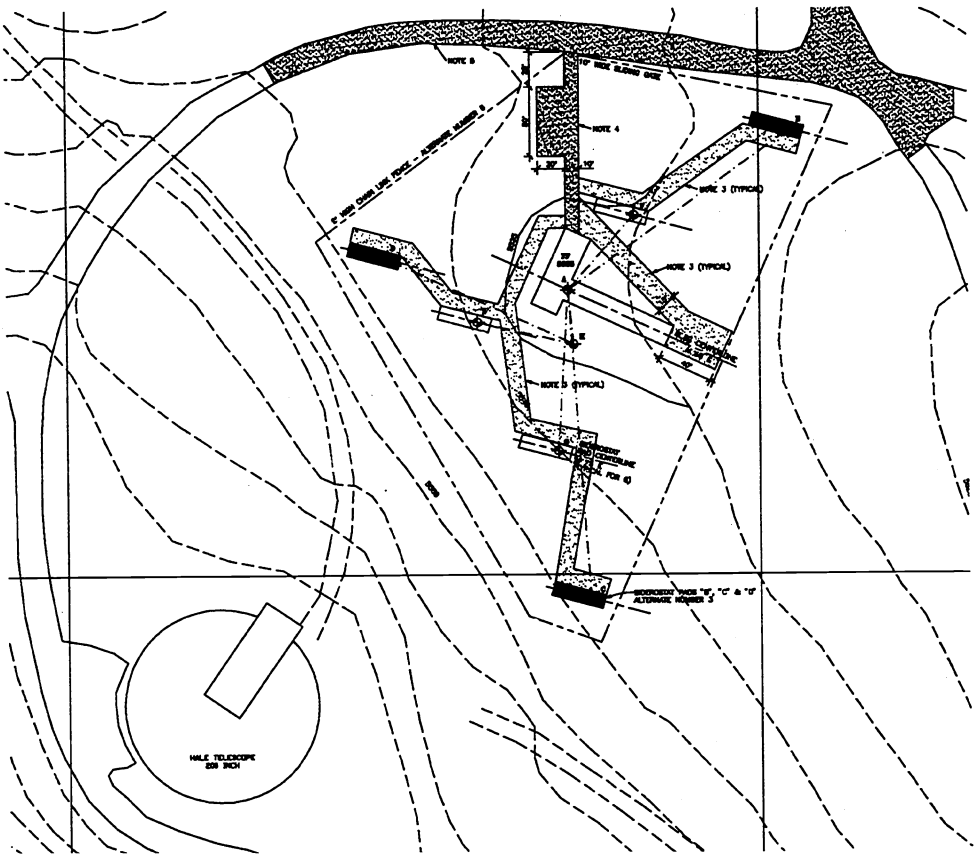

Figure 2: Testbed location at Palomar Mountain

are ~100 m. The central building, shown in Fig. 3, comprises a long section containing the long optical delay lines. The top section of the building contains the beam combiners, short delay lines, and beam compressors, as shown in Fig. 4. In addition, a partitioned-off computer room is available for real-time computers and electronics. At infrared wavelengths, the dispersion problems which necessitate the use of vacuum pipes at shorter wavelengths are not present, and the delay lines (and the whole instrument) will operate in air. Structural insulating foam will be used to construct an enclosure around the optics and delay lines to minimize turbulence. For propagation outside of the building, simple beam enclosures (beyond short stubs already planned to avoid turbulence at the building interface) could be added if found necessary.

It is convenient to divide the interferometer into two major subsystems: the pointing system and the phasing system. The pointing system comprises those elements which collect and control the direction of the incoming wavefront, including the siderostats, acquisition system, dual-star feeds, and star tracker. The phasing system comprises those elements specific to fringe detection including the fringe trackers/beam combiners, optical delay lines, and laser metrology system.

2.1. Pointing system

Siderostat The two siderostats collect light from both the primary and secondary stars. Each siderostat is comprised of a 50 cm flat mirror in an alt-az gimbal mount. The drive system uses a servo motor with a 1000-line optical encoder followed by a 5:1 belt drive and 100:1 harmonic drive which drives the telescope via a 24:1 friction drive. Axis encoders with 7 arcsec resolution provide absolute pointing. The light collected by the siderostat feeds a 40 cm telescope as shown in Fig. 5; the 15^o down-looking attitude of the telescope improves the sky coverage. A corner reflector located near the telescope serves as a fiducial for the constant-term laser metrology system. The siderostat control system performs the expected open- and closed-loop tracking functions, and in addition,

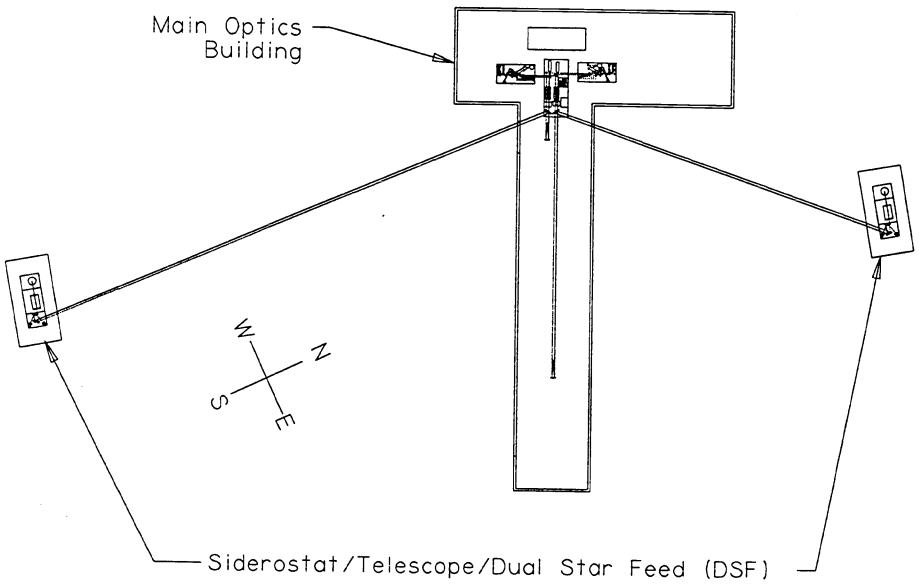

Figure 3: Testbed main building layout

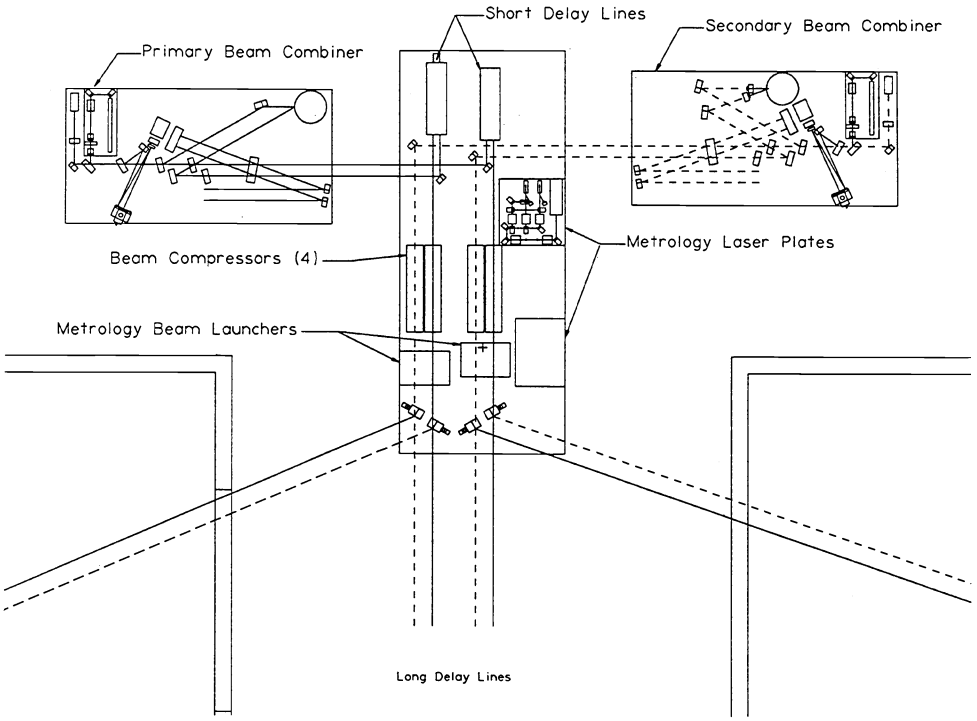

Figure 4: Testbed main building detail

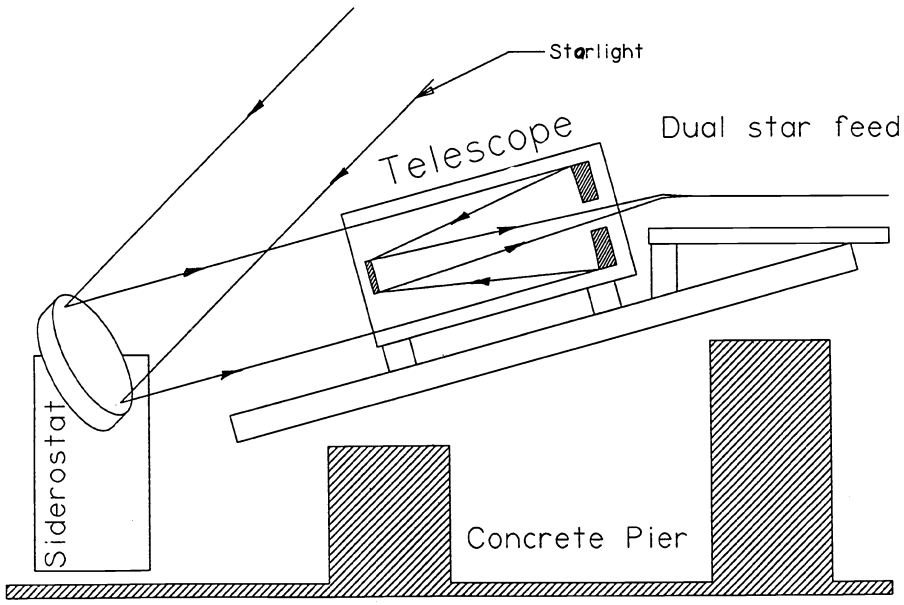

Figure 5: Siderostat, telescope, dual-star feed orientation

includes software to solve for the geometric mount model to improve open-loop pointing accuracy.

Acquisition system The function of the acquisition system is to bring the primary and secondary stars into the field of view of the star-tracker sensors located on the beam-combiner tables inside the main building. The acquisition system at each siderostat uses a CCD detector fed by a 9 cm telescope located optically in the shadow of the secondary of the main 40 cm telescope, and uses a CCD camera with a 12×17 arcmin field of view. The feed optics for the acquisition system include a corner cube which directs boresight lasers from the two beam combiners into the acquisition camera. The boresight laser from the primary beam combiner establishes the main instrument boresight. The boresight laser from the secondary beam combiner encodes the position of the secondary star selector mirror, discussed below. The functions performed by the acquisition system include alignment of the field separator in the dual-star feed and acquisition and centering of the primary star onto the instrument boresight by commanding the siderostat. In addition, the acquisition system centers the secondary star by commanding the secondary star selector mirror to move the star image onto the secondary laser boresight (bright case) or to move the secondary laser boresight onto the expected secondary star location (faint case).

Dual-star feed The dual-star feed separates the light from the primary and secondary stars and outputs collimated beams to the central building. A schematic of the dual-star feed is shown in Fig. 6. The 40 cm telescope shown in Fig. 5 forms an f/10 image of the field on a field separator—essentially, a coronagraphic stop. The light from the primary star transmits through the hole in the stop, is recollimated by a parabolic mirror, reflects off the annular mirror, and is directed by a steering mirror toward the main building. The remainder of the field reflects from the stop and is similarly recollimated. The final mirror in the secondary chain is the secondary star selector mirror. This motorized mount is located at a pupil (siderostat image) and is used to select a reference star nearby the target star. (From a control point of view, the secondary star selector mirror is treated like another siderostat, and is controlled by the siderostat controller.) The field of view of the dual-star feed is approximate ± 5 arcmin, limited by vignetting on the annular mirror, and the output beam size propagated to the central building is 7.5 cm. The parabolic mirror mounts are PZT actuated over small angles for tip/tilt control, and receive feedback signals from the star tracker.

Star tracker The star tracker maintains accurate parallelism between the interfering wavefronts in each beam combiner in order to maintain high fringe visibility. The sensor for each star tracker is a quad cell implemented

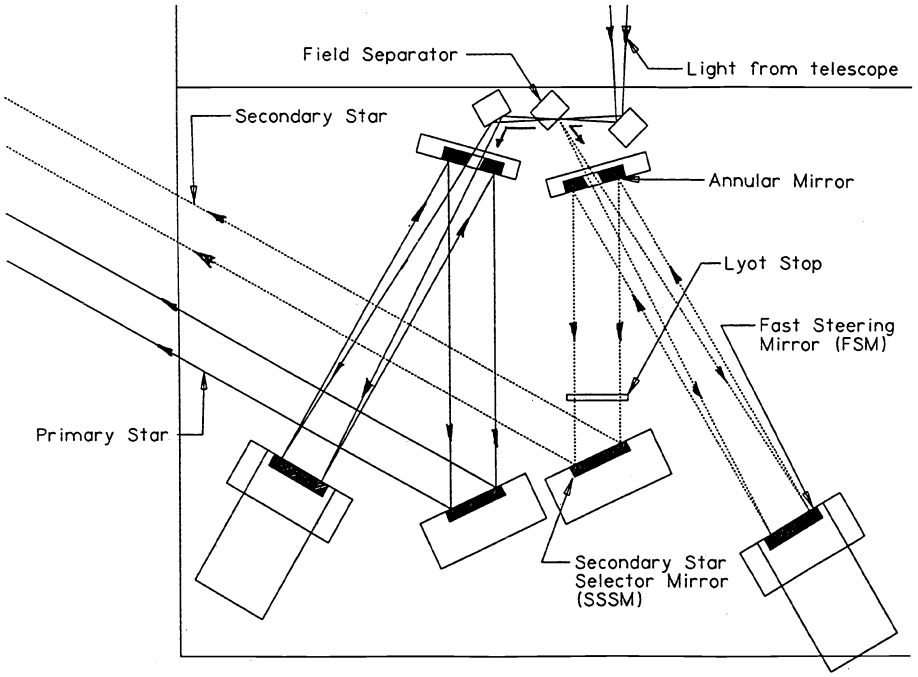

Figure 6: Dual-star feed

using a micro-lenslet array feeding four fiber-coupled photon-counting APD detectors. A single quad cell is employed in each beam combiner, with a PZT chopper mirror selecting between images of the two input beams. The chopper period is nominally 10 ms: ~5 ms on each image, with a small amount of dead time for settling. A dichroic beamsplitter in the beam combiner reflects the 0.7–1.0 μm band for star tracking; the short cutoff is to avoid scattered light from the laser metrology system, while the long cutoff is due to the bandgap of the silicon detectors. The APDs have a quantum efficiency of ~25% at 830 nm, and all have dark counts of less than 5 counts/s. The functions performed by the star tracker include high bandwidth tracking on the bright primary star (10 Hz closed-loop bandwidth, appropriate for these aperture sizes); low bandwidth tracking on the faint secondary star; and feedforward of the high frequency tilt information from the primary star to the secondary star for an isoplanatic tilt correction. The star tracker also includes a boresight mode to establish the zero points of the trackers, accomplished by setting the extremes of the chop range.

2.2. Phasing System

Primary fringe tracker This beam combiner and fringe tracker measures the fringe parameters for the bright primary star. For fringe tracking, it must read out faster than the atmospheric coherence time. For 1 arcsec seeing, τ_0 at 2.2 μm is ~50 ms; to allow for acceptable fringe unwrapping, the coherent integration time is set at 10 ms. Fringe encoding uses pathlength modulation, similar to the Mark III, with all of the light from 2.0–2.4 μm from one side beamsplitter focused onto a single pixel of a NICMOS-III infrared array detector. Light from the other side of the beamsplitter passes through a low resolution spectrometer and is imaged adjacent to the white-light spot onto the same line of the NICMOS chip. This line is then read out repeatedly: each frame starts with a reset, a delay to allow for reset settling, a read of the reset level, and then 4 reads separated by pathlength modulation changes of $\lambda/4$. While the system employs commercial front-end electronics, the clocking is accomplished with custom electronics to allow for varying the array timing for the spectrometer pixels in order to match the stroke to the wavelength, as well as to implement multiple reads to reduce the effective read noise of the chip. For our system, we are achieving an effective read noise of <20 e^-. The fringe phase measured on the white-light channel is the primary observable in this beam combiner. It is used to feed back to the long delay line to track out atmospheric turbulence. The spectral information from this beam combiner provides not only

visibility as a function of wavelength, but also allows for unambiguous identification of the central fringe.

Secondary fringe tracker This beam combiner and fringe tracker measures the fringe parameters for the faint secondary star. As this beam combiner is cophased using the phase information from the primary fringe tracker, long coherent integration times can be used so that read noise no longer dominates, and SNR is instead dominated by the noise from the thermal background and OH airglow. For long integrations, pathlength modulation cannot be used, and instead a dispersed fringe technique is used. Briefly, the spectrometer disperses the combined light across ~80 pixels over the K band. With a fixed pathlength offset, the measured intensity will vary sinusoidally as a function of wavenumber with peaks where the pathlength offset is evenly divisible by the wavelength. The location of the peak of the Fourier transform of this pattern is the group delay, i.e., the position of the white-light fringe. As background is important in this system, the spectrometer will be fully cryogenic.

Delay lines The delay lines in the testbed provide pathlength control to remove the sidereal motion of the fringes as well as to track out the atmospheric error measured by the primary fringe tracker. The testbed uses 4 delay lines, two long and two short. Each long delay line is physically 20 m long, providing a total delay range of ±40 m. As only the difference in the position of these two delay lines matters, only one is fully active, while the other uses just a motor. The design is similar to those developed at JPL for use by the Navy Prototype Optical Interferometer.[5] These delay lines delay both the primary and secondary star beams; thus feedback to these delay lines from the primary fringe tracker serves to cophase the instrument. There are also two short delay lines, one fixed, and one with a physical range of 20 cm, which serve to offset the pointing of the interferometer baseline from the primary star to the secondary one. The short delay lines are inserted in the primary star beam train, where they also serve as the source of the pathlength modulation used in the primary beam combiner. The long delay lines have a dedicated heterodyne metrology system of a fairly conventional design (similar to what was used on the Mark III), while the feedback signals for the short delay lines come from the constant-term metrology system. Between the two sets of delay lines are beam compressors which reduce the 7.5 cm beams from the dual-star feeds to 2.0 cm for input to the short delay lines and beam combiners.

Constant-term metrology The primary goal of the constant-term metrology system is to control systematic errors within the instrument to enable narrow-angle astrometry at the atmospheric limit. Because of the high precision required—10 nm of pathlength accuracy corresponds to 20 μas on a 100 m baseline—it is necessary to monitor the entire optical train fully common mode with the starlight. To this end, for each beam combiner, a low-frequency heterodyne metrology beam is inserted into a part of the starlight pupil exiting from one side of the main beamsplitter. This beam propagates backwards through the system, is split by the beamsplitter, and separate polarizers in each arm select the s polarization for one arm and the p polarization for the other. These individual polarizations then propagate through the entire optical train to a corner cube located in front of each siderostat. For the narrow fields of view over which high accuracy must be maintained, it is not necessary for the corner cube to be located on the siderostat mirror. To first order, for a field of 0.1 mrad (20 arcsec), and a required metrology accuracy of 10 nm, this configuration is acceptable as long as the deviations of the siderostat from an ideal gimbal are less than 100 μm, which is easily achieved. From the corner cubes, the metrology beams retroreflect through the system, are combined at the starlight beamsplitter, and the beat is detected with a photodetector. This scheme is not especially light-efficient, but through the use of a low heterodyne frequency, there is adequate signal-to-noise ratio.

The metrology is calibrated by adjusting the dual-star feed so that both primary and secondary beam combiners can observe the primary star. The pinhole used as a field separator is actually implemented as a reflective annulus deposited on a substrate which is a few percent reflective at 2.2 μm and ~50% reflective at 633 nm, so that the secondary star selector mirror can select an attenuated version of the primary star while maintaining continuity of the secondary metrology.

Finally, the constant-term metrology system includes provision to frequency shift the laser output by up to 40 MHz, which with $\lambda/256$ precision in the measurement of the metrology phase, allows for absolute metrology at the cm level, greatly simplifying initial acquisition of fringes.

2.3. Computer system

A key aspect of the successful operation of an interferometer is the integration of various subsystems with their specific computer control systems, as well the integration of the various subsystems with each other and the overall instrument controller. The control architecture for the testbed is based on VME hardware and 680x0 single-board computers running VxWorks, with overall instrument control and user interface implemented on a Sun workstation. The system uses three VME crates: one for the fringe trackers (2 CPUs), one for the delay lines (3 CPUs), and one for the siderostats (1 CPU), acquisition system (1 CPU), and star trackers (1 CPU). While not all of these systems need the full horsepower of a single CPU, the partitioning of functions greatly eases systems integration. The third VME crate includes fiberoptic bus repeaters to connect to small slave crates located at each siderostat shelter containing interface boards for controlling the siderostat and secondary star selector mirrors, the PZT mirrors, and the acquisition cameras. Additionally, the third crate contains a CPU used for running a realtime sequencer. A reflective memory provides inter-CPU communications among the three main VME crates.

A common communications architecture was developed using the reflective memory among card cages together with RPCs between the card cages and the Sun; a goal was to make the underlying transport mechanism transparent to the subsystem developers. Common software for communicating between subsystems and the sequencer, and for generating error, status, and data recording streams, is used by each subsystem. In addition, there are common utilities for initialization, real-time scheduling of tasks, and other functions. For more detail, see the accompanying paper.[6]

3. PROJECTED PERFORMANCE

For a 100-m baseline and a 15-arcsec star separation, we expect to achieve an atmospherically-limited accuracy of $\sim$30 μas in one hour of integration. Our goal is to control systematic errors in order to yield astrometric accuracies of $<$60 μas. The projected sensitivity of the system is estimated as K = 6–7 for the primary star (equivalent to V = 9–10 for a K5 spectral type), limited by the detector read noise. For the secondary star, where phase-referencing allows for long integration times, we estimate a signal-to-noise ratio of 5 should be obtainable in 1000 s for stars as faint at K = 13–14 (equivalent to V = 16–17 for a K5 spectral type), limited by optics emissivity and OH airglow. For the angle trackers, we estimate limiting magnitudes for high-speed (10 Hz) tracking on the primary star of R = 12–13, and for low-speed (0.1 Hz) tracking on the secondary star of R = 16–17, so that the fringe tracker should always establish the limiting magnitude. With performance of this level, in addition to demonstrating system operation of an instrument to perform high accuracy narrow-angle astrometry, an astrometric search program could be commenced around some nearby stars in order to look for Jupiter- and Saturn-mass planets. Compared to the Keck Interferometer, the major compromise with the testbed is lower sensitivity, mostly due to the small apertures employed. This translates into a smaller fraction of targets for which suitable astrometric reference stars can be found. The Keck Interferometer, in addition to providing higher accuracy due to the better seeing at Mauna Kea, with its much higher sensitivity and larger isoplanatic patch should be able to find reference stars nearby most targets.

4. CONCLUSION

At present, many of the subsystems of the testbed interferometer are working stand-alone in our laboratory, with integration of the various subsystems the next major objective. Site development at Palomar Mountain is planned for 1994, with installation later in that year, and initial operation in 1995. Given successful operation of the testbed, we hope in the future to augment its capabilities to demonstrate the technology for phase-referenced imaging with multiple telescopes for high sensitivity on faint, extended infrared targets; this is another key technology for the Keck Interferometer. In addition, we hope to conduct a preparatory science program to establish an observational baseline toward a search for exoplanets and to gain experience with the new observational modes.

5. ACKNOWLEDGEMENTS

Thanks to Kadri Vural and Rockwell International for help with the NICMOS-III detectors. This work is funded by the Solar System Exploration Division of NASA. This work was performed at the Jet Propulsion Laboratory, California Institute of Technology, under a contract with the National Aeronautics and Space Administration.

References

1. M. Shao and M. M. Colavita. Potential of long-baseline infrared interferometry for narrow-angle astrometry. *Astron. and Astrophys.*, 262:353–358, 1992.

2. M. M. Colavita. Measurement of the atmospheric limit to narrow-angle interferometric astrometry using the Mark III stellar interferometer. *Astron. and Astrophys.*, in press, 1994.

3. M. Shao, M. M. Colavita, B. E. Hines, D. H. Staelin, D. J. Hutter, K. J. Johnston, D. Mozurkewich, R. S. Simon, J. L. Hershey, J. A. Hughes, and G. H. Kaplan. The Mark III stellar interferometer. *Astron. Astrophys.*, 193:357–371, 1988.

4. M. Shao and M. M. Colavita. Long-baseline optical and infrared stellar interferometry. *Annu. Rev. Astron. Astrophys.*, 30:457–498, 1992.

5. M. M. Colavita, B. E. Hines, M. Shao, G. J. Klose, and B. V. Gibson. Prototype high speed optical delay line for stellar interferometry. *Proc. SPIE*, 1542:205–212, 1991.

6. B. E. Hines. ASEPS-0 testbed interferometer control system. *Proc. SPIE*, 2200:this proceedings, 1994.